Electron Transport through Single Molecules: Scattering Treatment Using Density Functional and Green Function Theories

Pedro A. Derosa and Jorge M. Seminario*

Department of Chemistry and Biochemistry, University of South Carolina, Columbia, South Carolina 29208

Received: August 23, 2000

Green function and density functional theories are used to study electron transport characteristics through single molecules addressed by two metallic contacts. Each contact is modeled with one nanoscopic end connected to the molecule and one macroscopic end connected to an external potential difference. The method can be applied to any molecular system for which ab initio calculations can be performed. It allows us to determine the molecular orbitals participating in the electron-transfer process, the current−voltage characteristics of the junction, the density of states, and the transmission function, among other properties, providing a fundamental tool for the development of molecular electronics. The method is tested with $Au_n-S-(p\text{-}C_6H_4)-S-Au_n$ ($n = 1-5$) connected to bulk gold. Current−voltage characteristics are in excellent agreement with a break junction experiment and with other ab initio calculations, yielding new insights regarding electron transport through single molecules.

Introduction

The study of electron transport in metal−molecule−metal interfaces is a fundamental step in the development of molecular electronics in particular and nanotechnology in general.[1] The influence of the metal and its defects on the properties of molecules attached to them has greater impact than the corresponding effects at interfaces in present electronic devices.[2,3] This is because single molecules yield a less robust band structure than semiconductors do. The transport of one electron through a single molecule induces a radical change in the electrical characteristics of the molecule. Therefore, standard mesoscopic techniques cannot be used without a complete description of the molecular system. This is true even for the qualitative determination of electron transport characteristics in present mesoscopic systems.[2,3]

Measurements of single molecules are needed proof-of-concept for the field of molecular electronics. The need to test whether single molecules can act as active electronic devices compels us to connect single molecules to macroscopic probes. This allows us to prove the concept but also allows us to determine their current−voltage ($I-V$) characteristics, which are needed for the design and construction of useful systems. This is a strong experimental challenge, such as having two metallic tips within 10 Å in order to access two different sites in a single molecule. So far only one experiment of this kind has been reported,[4] and it has been described theoretically using a perturbational approach.[5] In addition, a device where three tips are connected to a single molecule is still a practical and technical challenge. However, molecule−molecule chemical bonds can be used to connect a large number of functional systems reaching sizes that can be easily addressed by the standard microelectronics techniques. Fortunately, the inevitable task of obtaining electrical characteristics of single molecules can be performed precisely using present quantum chemistry techniques, which are becoming a substantial tool for the development of molecular electronics. Quantum chemistry can be used efficiently for the design of molecular electronic devices substituting difficult experiments involving two or more contacts.

Several experiments have been performed which self-assemble molecules on a metallic substrate and sample the conductance of these molecules with a scanning tunneling microscope (STM).[6−9] Other experiments were performed depositing a second contact over the self-assembled molecules.[10,11] In the latter, a cluster of ca. 1000 molecules can be addressed in parallel. If conditions are such that interactions between the N molecules are avoided during the self-assembly process, it can be considered that the measurements for the fabricated nanopore correspond to N times the measurement of a single molecule. On the theoretical front, DFT calculations combined with molecular dynamics simulations were used to explain experimental conductance characteristics observed in a thiotolane monolayer.[12] Several aspects of the resistance in a line of a few atoms,[13−15] and the $I-V$ characteristic of $S-(p\text{-}C_6H_4)-S$ coupled to two contacts represented by a jellium model were also studied.[16] The study of conductance in molecules and molecular wires using Green function techniques has also been performed,[17−20] providing qualitative insight on electron transport. It has been shown that the analysis of just a few atoms of a system provides information needed to explain certain macroscopic effects,[21] supporting the assumption that local effects are most important when electrical properties are of interest.

The effects of metallic tips connecting the molecule need to be evaluated in order to obtain precise quantitative predictions of chemical accuracy. A scattering formalism for mesoscopic conductors, developed by several groups,[22−28] is used in this work to describe the interaction of the molecule with the continuum (contacts). A Kohn−Sham (KS) Hamiltonian is used to analyze the electron transport properties of $S-(p\text{-}C_6H_4)-S$ attached to 1−5 Au atoms at each end. The KS Hamiltonian includes the electron correlation and fully nonlocal exchange effects that are extremely relevant for single-molecule systems.

* Corresponding author. Fax: (803) 777-9521. E-mail: jorge@mail.chem.sc.edu.

10.1021/jp003033+ CCC: $20.00
Published on Web 12/13/2000

Formalism

The Hamiltonian matrix, used in this formalism for the molecular description, is obtained from quantum chemistry calculations where few metallic atoms are added to each end of the molecule of interest. In this way, the molecular electronic structure, and the coupling between the molecule and the contacts are well described. The macroscopic contacts located after few metal atoms of the interface are modeled with the Green function for an isolated semi-infinite media.[22,28] An approach related to the one described here was first introduced by Mujica and Ratner using a tight binding Hamiltonian,[25,26] and recently substituted by a Hartree−Fock Hamiltonian.[29] In this work, we use DFT Hamiltonians in conjunction with a modified formalism based on that presented by Datta.[17,22,23] As far as we know, this is the first implementation of DFT and Green function procedures for the study of electron transport, and no studies using a large number of Au atoms attached to the molecule have been performed using ab initio methods. On the semiempirical side, Emberly used an extended Hückel tight-binding approach,[30] which included several Au atoms attached to the molecule.

We focus our present study on a system with two semi-infinite contacts having a continuum of states or channels of *s*, *p*, and *d* (split into t_{2g} and e_g) character for electron transport and a molecule between with discrete channels or modes of conduction. The molecule is bonded to actual metallic atoms. The metallic (Au) atoms are also part of a bulk system representing the contacts. Electrons flow if they can leave one contact, get into one of the available channels in the molecule already affected by the contacts, and reach the other contact. Conduction can occur in both directions at any voltage, and the net current is given by the difference between the currents in both directions. The current of electrons with energy between E and $E + dE$ that flows from left to right (+) and vice versa (−), on the left (1) and right (2) contacts is

$$i_1^+(E) = \left(\frac{2e}{h}\right) M(E) f_1(E)\, \mathrm{d}E \tag{1}$$

and

$$i_2^-(E) = \left(\frac{2e}{h}\right) M(E) f_2(E)\, \mathrm{d}E \tag{2}$$

where $M(E)$ is the number of transport channels that one electron with energy E can reach and $f_i(E)$ is the Fermi-Dirac distribution. The number of electrons coming out from the molecule to the contacts is given by two contributions, the electrons that effectively made it through the molecule and the electrons originated in the same contact that were backscattered, i.e.,

$$i_2^+(E) = \bar{T}(E) i_1^+(E) + (1 - \bar{T}(E)) i_2^-(E) \tag{3}$$

and

$$i_1^-(E) = (1 - \bar{T}(E)) i_1^+(E) + \bar{T}(E) i_2^-(E) \tag{4}$$

where $\bar{T}(E)$ is the transmission coefficient (probability per transport channel). Considering that electrons are neither removed nor attached to the molecule, $i^+ - i^-$ should be equal in both sides. Using eqs 1−4 and integrating in energy yields the current,

$$I(V) = \frac{2e}{h} \int_{-\infty}^{\infty} \mathrm{d}E\; T(E,V)[f_1(E,V_1) - f_2(E,V_2)] \tag{5}$$

The bias voltage $V = V_2 - V_1$ is now implicitly included in the distribution f_i. The transmission function is defined as

$$T(E) = \bar{T}(E) M(E) \tag{6}$$

The differential conductance can be calculated from eq 5 as

$$g = \frac{\partial I(V)}{\partial V} \tag{7}$$

The transmission function T can be calculated using the Green function technique:[22]

$$T(E) = Trace(\Gamma_1 G_M \Gamma_2 G_M^+) \tag{8}$$

Γ_i describes the coupling at the contact i. G_M is the retarded Green function for the molecule including the effect of the contacts and G_M^+ is its adjoint. The problem reduces to obtain a valid Green function for the molecule connected to the two semi-infinite metallic contacts. The Green function G for the whole system in matrix form has infinite dimensions; however, it can be partitioned into a form that allows us to use finite matrixes as follows:[22]

$$G(E) = \begin{bmatrix} g_1^{-1} & -\tau_1 & 0 \\ -\tau_1^+ & E1 - H_C & -\tau_2^+ \\ 0 & -\tau_2 & g_2^{-1} \end{bmatrix}^{-1} = \begin{bmatrix} G_1 & G_{1M} & G_{12} \\ G_{M1} & G_M & G_{2M} \\ G_{21} & G_{M2} & G_2 \end{bmatrix} \tag{9}$$

The submatrixes G and g represent Green functions when interactions among subsystems are included or excluded, respectively. g_i represents the contacts and τ_i describe the metal−molecule coupling. H_C is the Hamiltonian of the isolated molecule and E is the electron energy. Therefore, solving eq 9 for G_M, we obtain

$$G_M = [E1 - H_C - \Sigma_1 - \Sigma_2]^{-1} \tag{10}$$

where

$$\Sigma_1 = \tau_1^+ g_1 \tau_1 \tag{11}$$

and

$$\Sigma_2 = \tau_2^+ g_2 \tau_2 \tag{12}$$

Σ_i are the self-energy terms accounting for the interaction between the molecule and the contacts.

Quantum chemistry techniques can be used to obtain the elements needed for eqs 10−12. In our particular case, we use a KS Hamiltonian from a calculation that includes the molecule of interest and up to ten Au atoms representing the two metallic contacts. The calculated KS Hamiltonian in the atomic basis set can be partitioned as

$$H_{KS} = \begin{bmatrix} H_{11} & H_{1M} & H_{12} \\ H_{M1} & H_{MM} & H_{M2} \\ H_{21} & H_{2M} & H_{22} \end{bmatrix} \tag{13}$$

where the subscripts 1 and *2* refer to the contacts and *M* to the molecule. H_{KS} written in its canonical representation allows maximum delocalization of the molecular orbitals (MOs), providing a reasonable description of the coupling matrixes, and yielding valid comparisons among several systems. H_{MM} is

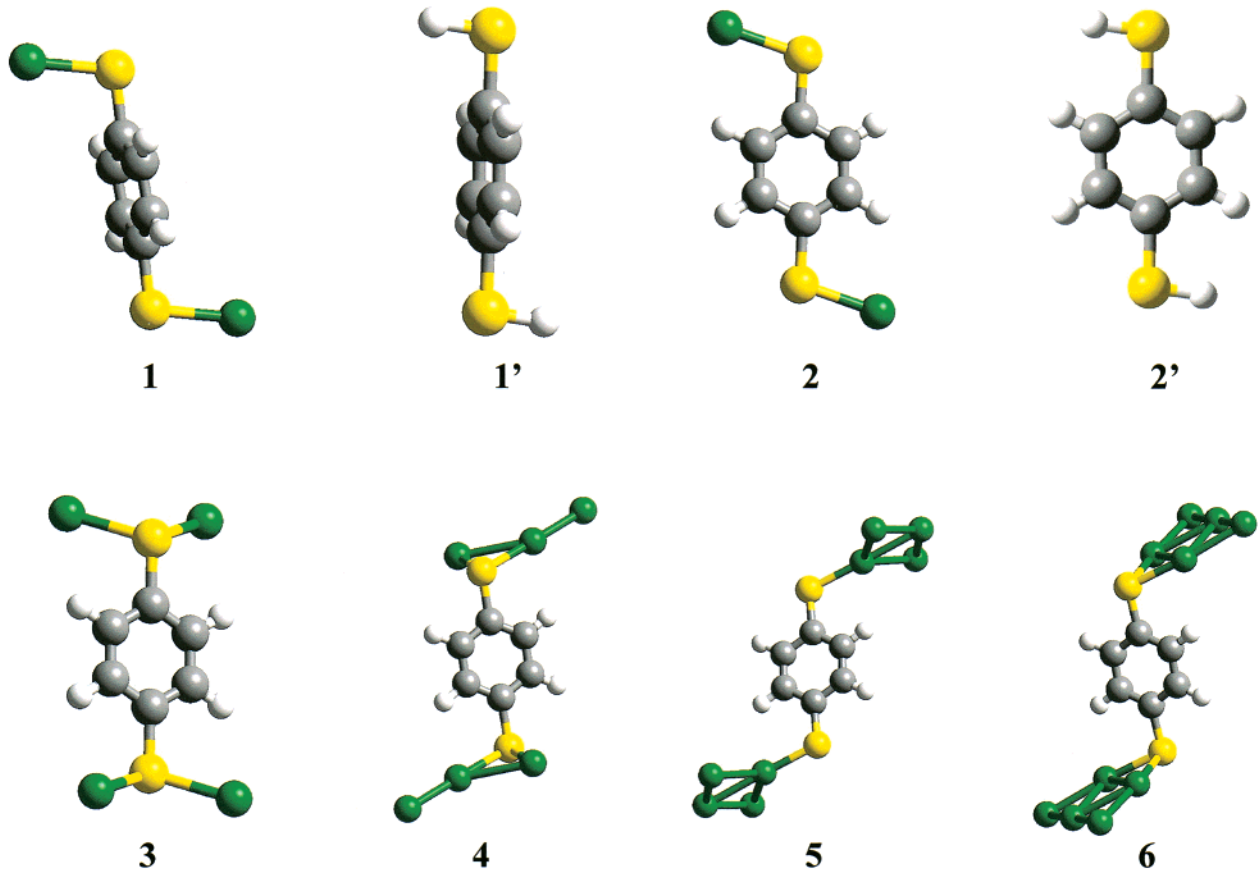

Figure 1. (**1**) Nonplanar Au−S−(*p*-C_6H_4)−S−Au system with Au atoms out of the benzene plane. (**2**) Planar Au−S−(*p*-C_6H_4)−S−Au. (**3**) Au_2−S−(*p*-C_6H_4)−S−Au_2. (**4**) Au_3−S−(*p*-C_6H_4)−S−Au_3. (**5**) Au_4−S−(*p*-C_6H_4)−S−Au_4. (**6**) Au_5−S−(*p*-C_6H_4)−S−Au_5. (**1′**) Nonplanar H−S−(*p*-C_6H_4)−S−H. (**2′**) Planar H−S−(*p*-C_6H_4)−S−H.

assigned to H_C in eq 9. H_{iM} and H_{Mi} are assigned to τ_i and τ_i^+, respectively, rendering a finite dimension case. Hypothetically, the coupling matrixes H_{iM} and H_{Mi} should represent the coupling to a geometrically and electronically perfect continuum; however, in real situations such as the break junction experiment,[4] the molecule is connected through a nanoscopic tip. Our ab initio studies also show that the tip atoms tend to arrange in planar structures that include the S atom as shown in Figure 1. To adapt this procedure to real conditions, a coupling factor was usually used as a fitting parameter,[28] affecting the coupling matrixes H_{Mi} and H_{iM} and the corresponding elements in the overlap matrixes S_{Mi} and S_{iM}. A coupling factor of 0.5, adopted mainly on intuitive geometrical grounds, is used in all the calculations reported here. This indicates that the nanoscopic tip contacting the molecule, which includes few Au atoms, ends up in a planar shape, whose volume is about 50% of what it would be if the ideal continuum were able to hypothetically connect to the molecule. Therefore, the coupling factor of 0.5 indicates that half of the continuum is in direct contact with the extended molecule.

Equation 10 can be written as

$$G_M[E\mathbf{1} - H_M] = \mathbf{1} \tag{14}$$

where H_M is

$$H_M = H_{MM} - H_{M1}g_1H_{1M} - H_{M2}g_2H_{2M} \tag{15}$$

The g_i for Au can be approximated as a diagonal matrix with each element proportional to their local density of states.[28] Using results from a theoretical estimation,[31] we can write them as

$$g_s = -0.072\,\pi i\,\mathbf{1}\ 1/\text{eV-atom} \tag{16}$$

$$g_p = -0.0426\,\pi i\,\mathbf{1}\ 1/\text{eV-atom} \tag{17}$$

$$g_{t_{2g}} = -0.1286\,\pi i\,\mathbf{1}\ 1/\text{eV-atom} \tag{18}$$

$$g_{e_g} = -0.0492\,\pi i\,\mathbf{1}\ 1/\text{eV-atom} \tag{19}$$

and we considered that half of the local density of these states are available for a specific spin state as it has been recently pointed out.[27] The coupling between the contacts and the molecule used in eq 8 is given by

$$\Gamma_j = i[\Sigma_j - \Sigma_j^+] \quad j = 1, 2 \tag{20}$$

where Σ is the Hermitian conjugate self-energy matrix and Σ^+ is its adjoint. The eigenvalues of H_M (eq 15) are complex; their real part determines the peak positions in the density of states (DOS) and their imaginary part determines the peak widths. These peaks are shifted and broadened with respect to the eigenvalues of H_{MM}, which represents the molecule without coupling. The spectral function A of the system contact−molecule−contact is given by

$$A = i[G_M - G_M^+] \tag{21}$$

and its trace is the DOS of the same system.

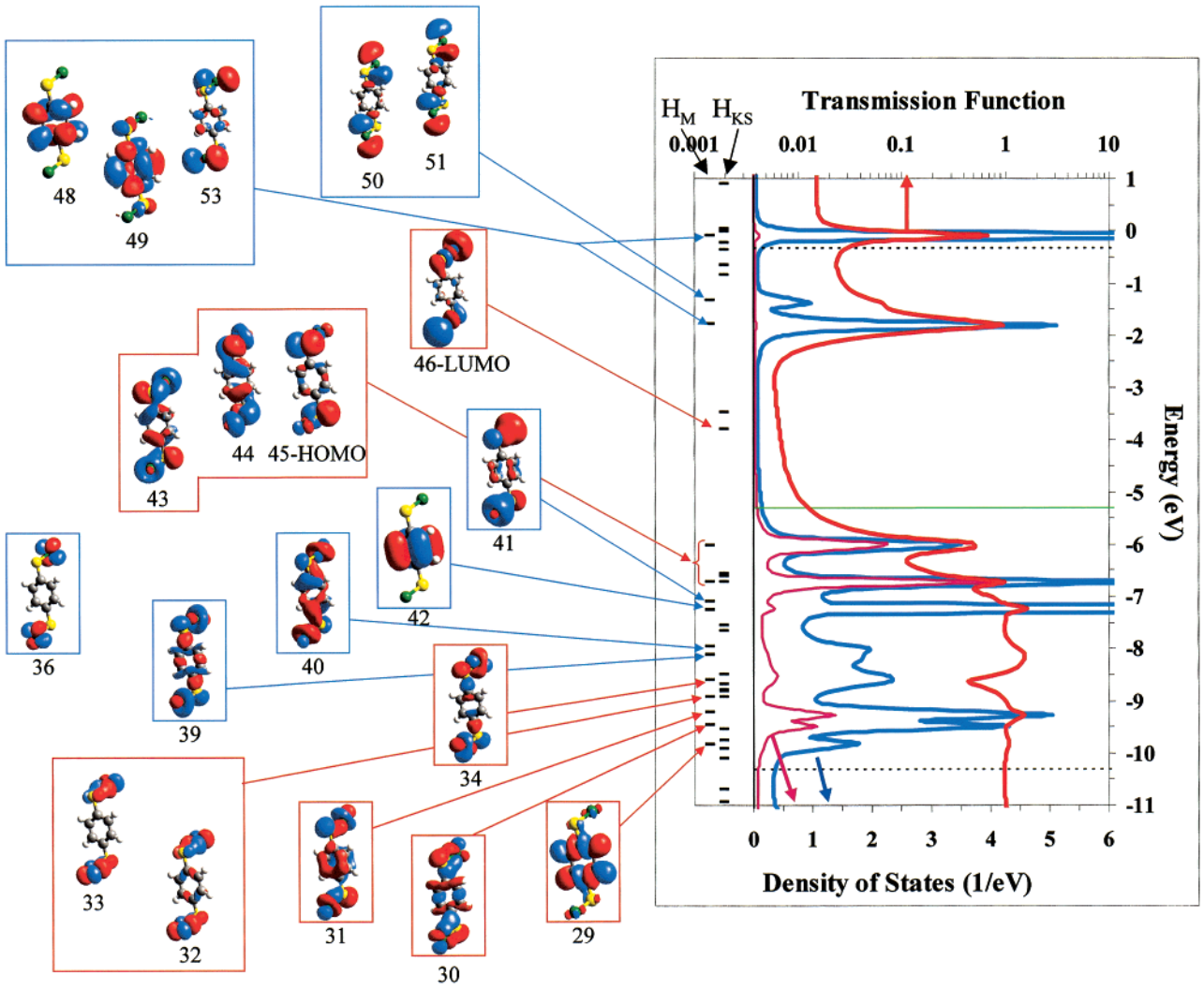

Figure 2. Density of states (blue curve), transmission function (red curve), and DOS projected on the S atomic orbitals (magenta curve) for Au−S−(*p*-C_6H_4)−S−Au with the Au atoms out of the benzene plane (**1**) and connected to an Au continuum, as a function of the incoming electron energy. The continuous green line indicates the position of μ (−5.31 eV for Au), i.e., the interface between the occupied and unoccupied levels. Relevant Kohn−Sham MOs are shown ordered with respect to their energies. MO 45 corresponds to the HOMO and MO 46 to the LUMO. The first set of bars corresponds to the eigenvalues of H_M (left) and the second set to the eigenvalues of H_{KS} (right). The arrows connect the H_{KM} MOs to the corresponding H_M eigenvalues.

Notice that the Green function solves a Schrödinger-like equation with source that corresponds to the eigenvalue problem $H\Psi = E\Psi$,[22] whereas the KS Hamiltonian allows us to solve the generalized eigenvalue equation

$$H_{KS}\Psi = \epsilon S\Psi \tag{22}$$

where S is the overlap matrix and ϵ are the eigenvalues. Thus, after applying the geometric coupling factor, previous to any further use of H_{KS}, we transform it as

$$H_{KS} \rightarrow S^{-1}H_{KS} \tag{23}$$

This transformed Hamiltonian is symmetrized in order to ensure hermiticity.[32] The submatrix H_{MM}, as well as H_{iM} and H_{Mi}, obtained from the transformed and symmetrized H_{KS}, comprehends the molecule and also its interaction with the metal atoms representing the contacts. This yields a description of the real physical process for the "molecule", which does not have a precisely defined boundary from the continuum; therefore, the first Au atoms contacting the molecule can also be considered part of the molecule. Actually, the metallic atoms close to the molecule behave more as part of the molecule rather than as part of the bulk system.

H_{KS} and S are obtained from a DFT geometry optimization at the B3PW91/LANL2DZ level of theory as implemented in Gaussian 94 and Gaussian 98 programs.[33,34] The B3PW91/LANL2DZ level of theory uses the Becke-3 hybrid exchange functional and the generalized-gradient approximation (GGA) Perdew−Wang 91 correlation functional,[35−37] with the LANL2DZ basis set.[38−40] The B3PW91/LANL2DZ has been successfully applied to other systems,[5,21,41−43] where the details of the calculations are explicitly discussed. The S−(*p*-C_6H_4)−S molecule attached to a few Au atoms was fully optimized under C_i symmetry; the resulting structures are shown in Figure 1, which also shows two conformations of HS−(*p*-C_6H_4)−SH used as reference to study the effects of Au atoms. The angle C−S−Au varies between 102° and 108° for all the cases. During the geometry optimization several initial configurations were tested; none converged to a linear geometry. Second derivative calculations were performed on the optimized structures yielding no negative eigenvalues of the Hessian matrix, confirming that the structures correspond to a local minima in the potential surface

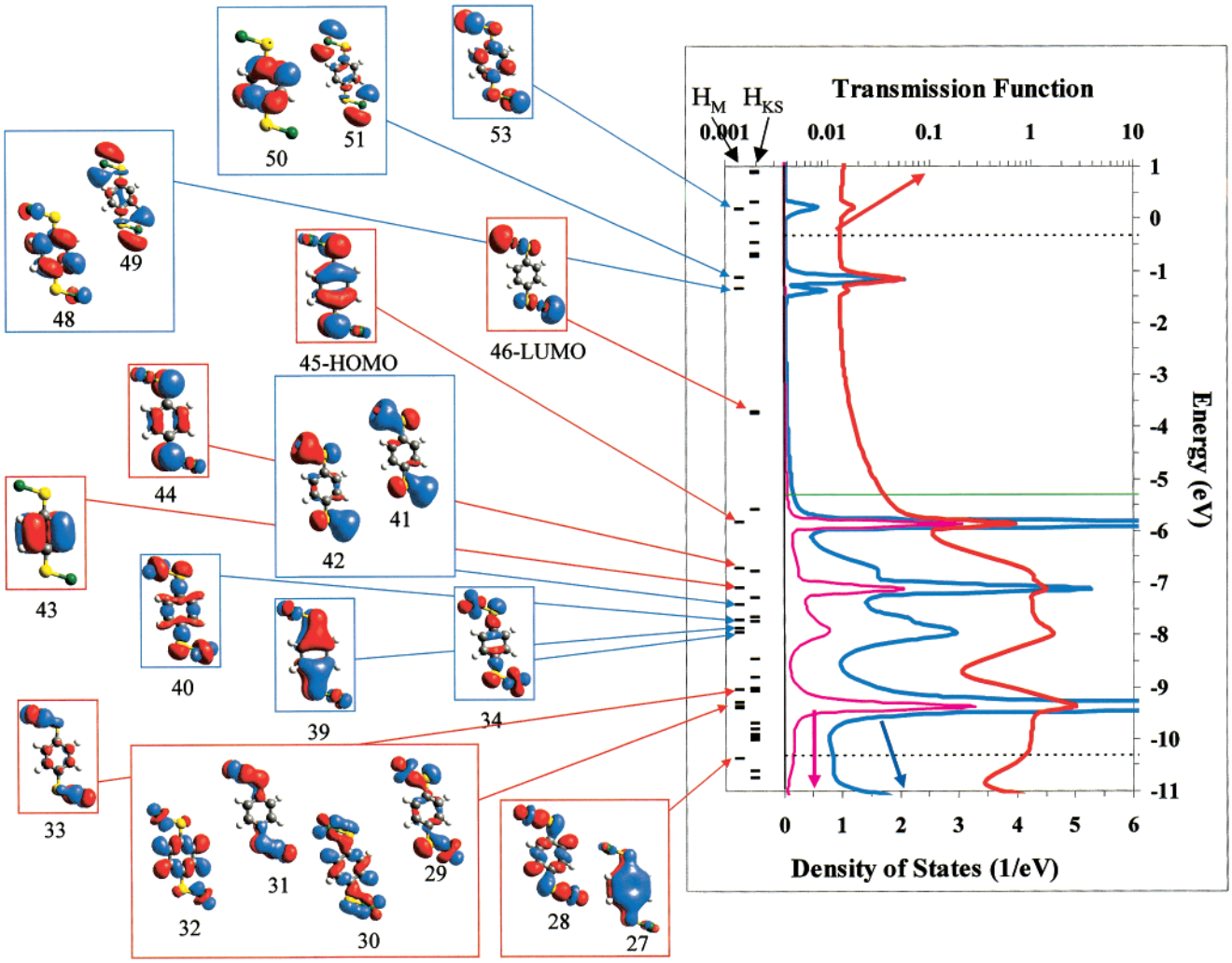

Figure 3. Same as Figure 2 for molecule **2**.

of $Au_n-S-(p\text{-}C_6H_4)-S-Au_n$ ($n = 1-5$). The chemical potential (μ) of the molecule is pinned to the Fermi level of the metal when no external field is applied. The Au (111) work function, -5.31 eV,[44] is used as the Fermi energy for the bulk Au at zero bias voltage and thus μ is not used as an adjustable parameter. The applied voltage shifts the Fermi level in the metal contacts (by E_{f1} and E_{f2}) up and down and the chemical potential of the molecule (μ) will relocate in between. This is equivalent to using the molecule's chemical potential (μ) as a reference level and the Fermi levels of the contacts warping upward and downward accordingly. This does not change the physics of the process and it is preferred for practical reasons; therefore,

$$E_{f1} = \mu - \frac{1}{2}eV \tag{24}$$

and

$$E_{f2} = \mu + \frac{1}{2}eV \tag{25}$$

define the energy limits for the calculation of the current.

Results and Analysis

Figure 1 shows the systems $Au_n-S-(p\text{-}C_6H_4)-S-Au_n$ ($n = 1-5$) treated in this work. For $n = 1$, two configurations were chosen: one with the Au atoms out of the benzene plane (**1**) and the other with the Au atoms on the plane (**2**). The latter was less stable by 5.75 kcal/mol; however, both were local minima. Figures 2 and 3 show for **1** and **2**, respectively, the DOS (blue), the transmission function (red), and the projection of the DOS on the S atomic orbitals (AOs) (magenta), as well as some of the KS MOs. The continuous horizontal line (green) indicates the position of μ and the dotted lines are drawn at ± 5 eV from μ. The DOS represents the discrete energy levels of the isolated molecule shifted and broadened by the presence of the infinite contacts. The eigenvalues of H_M directly determine the DOS and are represented by the left set of bars. The eigenvalues of H_{KS} are represented by the right set of bars and they correspond to the molecule with the Au atoms added at both ends.

The transmission function and the DOS are strongly correlated, especially in the location of their peaks; correlations between valleys and peaks can be also found. The transmission function practically defines the electrical properties of the system. Therefore, it is of great importance to be able to predict its features using the KS MOs, establishing a correspondence between the eigenvectors of H_{KS} with the eigenvectors of H_M, and thus with the peaks in the DOS and transmission function. In most cases the position of peaks in the DOS can be assigned to the eigenvalues of H_{KS}. However, these assignments are not always straightforward. There are cases when one eigenstate of H_M corresponds to more than one eigenstate of H_{KS} because of the mixing of Au AOs with the AOs of other atoms in the

TABLE 1: Mulliken Population Contributions (%) from the AOs to the Kohn−Sham MOs for 1 Using the B3PW91/LANL2DZ Procedure

	31	32	33	34	35	36	37	38	39	40	41	42
C_1,C_4 (*s*)	0.0	0.0	0.0	1.1	0.0	0.0	0.0	0.0	0.7	0.0	0.0	0.0
C_1,C_4 (*p*)	4.6	2.2	0.3	7.0	2.3	0.0	0.0	0.0	10.1	25.6	0.4	0.0
C_2,C_5 (*s*)	0.0	0.0	0.0	0.0	0.0	0.0	0.0	0.0	0.0	0.0	0.4	0.0
C_2,C_5 (*p*)	7.0	1.3	0.3	0.2	0.4	0.0	0.0	0.0	4.4	5.0	3.0	49.5
C_3,C_6 (*s*)	0.0	0.0	0.0	0.2	0.0	0.0	0.0	0.0	0.0	0.0	0.0	0.0
C_3,C_6 (*p*)	7.0	0.9	0.5	0.3	0.3	0.0	0.0	0.0	4.7	5.0	3.5	50.0
$S_{11}-S_{12}$ (*s*)	4.7	0.0	0.0	4.1	0.0	0.0	0.0	0.0	3.6	0.3	0.9	0.0
$S_{11}-S_{12}$ (*p*)	16.5	7.7	8.3	10.0	0.4	0.0	0.0	0.0	15.5	12.1	31.1	0.0
$Au_{13}-Au_{14}$ (*s*)	0.0	0.0	0.0	0.6	0.6	0.0	0.0	0.0	4.2	6.1	36.3	0.0
$Au_{13}-Au_{14}$ (*p*)	0.0	0.0	0.0	0.4	0.0	0.0	0.0	0.0	1.0	0.3	0.2	0.0
$Au_{13}-Au_{14}$ (*d*)	60.2	86.1	90.3	75.6	95.9	99.8	99.9	99.7	53.4	44.9	24.6	0.0

	43	44	HOMO	LUMO	47	48	49	50	51	52	53
C_1,C_4 (*s*)	0.0	0.0	0.0	0.0	0.0	0.0	0.0	0.0	0.6	0.0	0.0
C_1,C_4 (*p*)	17.6	18.2	2.1	2.6	2.0	0.2	51.5	3.5	7.1	0.0	0.0
C_2,C_5 (*s*)	0.0	0.0	0.3	0.0	0.0	0.0	0.0	0.0	0.3	0.0	0.0
C_2,C_5 (*p*)	3.2	5.5	1.3	2.1	1.6	40.6	17.9	0.3	1.2	0.0	5.3
C_3,C_6 (*s*)	0.3	0.0	0.0	0.0	0.0	0.0	0.0	0.0	0.0	0.0	0.0
C_3,C_6 (*p*)	5.1	3.1	1.7	1.9	1.9	47.1	10.4	0.0	1.9	0.0	6.1
$S_{11}-S_{12}$ (*s*)	0.7	0.6	0.0	0.0	0.0	0.0	0.0	0.7	0.4	0.0	0.0
$S_{11}-S_{12}$ (*p*)	47.8	47.3	82.2	21.2	29.6	0.0	5.7	7.5	6.1	1.6	1.4
$Au_{13}-Au_{14}$ (*s*)	17.9	17.1	0.0	54.6	44.7	0.0	0.3	0.0	0.0	0.0	0.0
$Au_{13}-Au_{14}$ (*p*)	1.3	1.3	2.7	12.6	14.7	11.7	12.7	87.4	83.5	97.7	87.7
$Au_{13}-Au_{14}$ (*d*)	7.5	6.5	9.6	4.6	5.3	0.0	0.2	0.0	0.0	0.0	0.0

molecule. In other cases, some of the eigenvalues of H_{KS} do not participate in the DOS, such us those with exclusive Au nature. The arrows in Figures 2 and 3 connect some of the KS MOs to their corresponding H_M eigenvalues. Completing this information, Tables 1 and 2 show the AO contribution (%) to several MOs, some of them illustrated in Figures 1 and 2, respectively. These contributions are obtained using a Mulliken population analysis,[45] which are good estimators of the degree of localization or delocalization of the MOs.

Analyzing from low to high energies in Figure 2, there is a group of three peaks in the DOS corresponding to fully delocalized MOs 29−31. Localized π MOs 32 and 33 yield the next H_M orbital with small contribution to the DOS due to the low contribution of the C AOs. However, this π H_M orbital with S *p* and Au *d* character present high transmission function. In contrast, MO 34 yields the next H_M orbital, which has higher contribution from the C atoms than the H_M orbital associated with MOs 32 and 33 has, and a σ antibonding between S and Au atoms (see Figure 2). Therefore, MO 34 yields a larger contribution to the DOS but a smaller contribution to the transmission function than the H_M orbital formed by MOs 32 and 33. The H_M orbitals related to MOs 32−34 show relatively high transmission due to the coupling between S and Au. However, they also show lower transmission than the two H_M orbitals with large peaks in the DOS related to MOs 31 and to MOs 39−40. MOs 31, 39, and 40 are more delocalized and distributed around the molecule and Au atoms (Table 1) than MOs 32−34; therefore, MOs 31, 39, and 40 poses higher transmission, despite the good coupling to the Au atoms from all these six MOs. MOs 35−38 (only 36 is shown in Figure 2) are fully localized on the Au atoms as shown in Table 1 and thus do not contribute to the DOS.

The next DOS peak, at −7.26 eV, is formed by the overlap of two H_M orbitals located at −7.25 eV and −7.10 eV, which are related to MOs 41 and 42. The position of the DOS peak, closer to the first H_M orbital than to the second, suggests that this first peak is mostly associated with MO 42, which is totally localized on the ring whereas the second H_M orbital is mostly related to MO 41. This inversion of sequence is due to the different shift of the two MOs under the presence of the bulk

TABLE 2: Mulliken Population Contributions (%) from the AOs to the Kohn−Sham MOs for 2 Using the B3PW91/LANL2DZ Procedure

	27	28	29	30	31	32	33	34	35
C_1,C_4 (*s*)	0.0	0.3	0.0	0.0	0.0	0.0	0.0	1.4	0.0
C_1,C_4 (*p*)	35.2	5.3	2.0	8.5	5.1	17.5	2.1	8.9	0.4
C_2,C_5 (*s*)	0.0	0.3	0.0	0.5	0.0	0.0	0.0	0.0	0.0
C_2,C_5 (*p*)	25.5	7.9	1.4	9.5	0.7	13.4	3.2	1.0	0.2
C_3,C_6 (*s*)	0.0	0.5	0.0	0.0	0.0	0.0	0.0	0.0	0.0
C_3,C_6 (*p*)	25.6	11.9	1.4	8.9	0.5	13.8	3.5	0.4	0.0
$S_{11}-S_{12}$ (*s*)	0.0	3.1	4.5	0.0	0.0	0.8	0.0	4.9	0.0
$S_{11}-S_{12}$ (*p*)	8.4	19.4	18.3	12.8	14.9	2.9	4.6	13.1	0.0
$Au_{13}-Au_{14}$ (*s*)	0.0	2.9	0.0	0.9	0.0	0.7	0.0	1.1	0.0
$Au_{13}-Au_{14}$ (*p*)	0.0	0.2	0.0	0.0	0.0	0.0	0.0	0.6	0.0
$Au_{13}-Au_{14}$ (*d*)	5.0	41.2	71.9	50.9	78.0	29.6	86.1	68.3	99.4

	36	37	38	39	40	41	42	43	44
C_1,C_4 (*s*)	0.0	0.0	0.0	0.9	0.0	0.0	0.0	0.0	0.0
C_1,C_4 (*p*)	1.5	0.0	0.0	9.9	43.5	2.5	0.7	0.0	0.8
C_2,C_5 (*s*)	0.0	0.0	0.0	0.0	0.0	0.5	0.2	0.0	0.0
C_2,C_5 (*p*)	1.3	0.0	0.3	5.1	5.9	0.3	0.9	51.6	6.1
C_3,C_6 (*s*)	0.0	0.0	0.0	0.0	0.0	0.3	0.0	0.0	0.0
C_3,C_6 (*p*)	0.5	0.0	0.0	5.8	8.2	0.0	1.2	48.1	5.2
$S_{11}-S_{12}$ (*s*)	0.5	0.0	0.0	2.8	0.0	1.4	1.3	0.0	0.0
$S_{11}-S_{12}$ (*p*)	1.9	0.0	0.0	18.2	23.1	38.6	35.3	0.0	76.6
$Au_{13}-Au_{14}$ (*s*)	0.5	0.0	0.0	4.7	0.0	34.5	40.0	0.0	0.0
$Au_{13}-Au_{14}$ (*p*)	0.0	0.0	0.0	0.8	0.7	0.4	0.3	0.0	2.6
$Au_{13}-Au_{14}$ (*d*)	92.4	99.9	99.3	49.0	19.3	21.6	19.7	0.0	9.3

	HOMO	LUMO	47	48	49	50	51	52	53
C_1,C_4 (*s*)	0.0	0.0	0.0	0.0	1.2	0.0	1.2	0.0	0.0
C_1,C_4 (*p*)	19.6	0.5	1.7	10.0	5.9	31.5	4.1	0.0	18.7
C_2,C_5 (*s*)	0.0	0.0	0.0	0.0	0.0	0.0	0.0	0.0	0.0
C_2,C_5 (*p*)	7.8	0.5	0.4	45.1	1.7	2.3	0.0	0.9	18.2
C_3,C_6 (*s*)	0.0	0.0	0.0	0.0	0.0	0.0	0.0	0.0	0.0
C_3,C_6 (*p*)	9.7	0.4	0.3	9.9	0.6	56.5	0.0	0.7	0.0
$S_{11}-S_{12}$ (*s*)	0.0	0.0	0.0	0.0	0.5	0.0	0.6	0.0	0.0
$S_{11}-S_{12}$ (*p*)	56.9	26.8	25.4	0.0	9.0	2.5	5.5	1.6	5.8
$Au_{13}-Au_{14}$ (*s*)	0.0	49.4	50.2	0.0	0.0	0.0	0.0	0.0	0.0
$Au_{13}-Au_{14}$ (*p*)	2.6	16.5	16.8	32.9	79.1	7.3	90.6	96.8	59.3
$Au_{13}-Au_{14}$ (*d*)	3.7	5.2	4.8	0.0	0.0	0.0	0.0	0.0	0.6

Au. The large transmittance suggests a collective effect of MOs 41 and 42. MO 41 provides the connection to the Au, while MO 42 extends the delocalization to the ring. Due to the

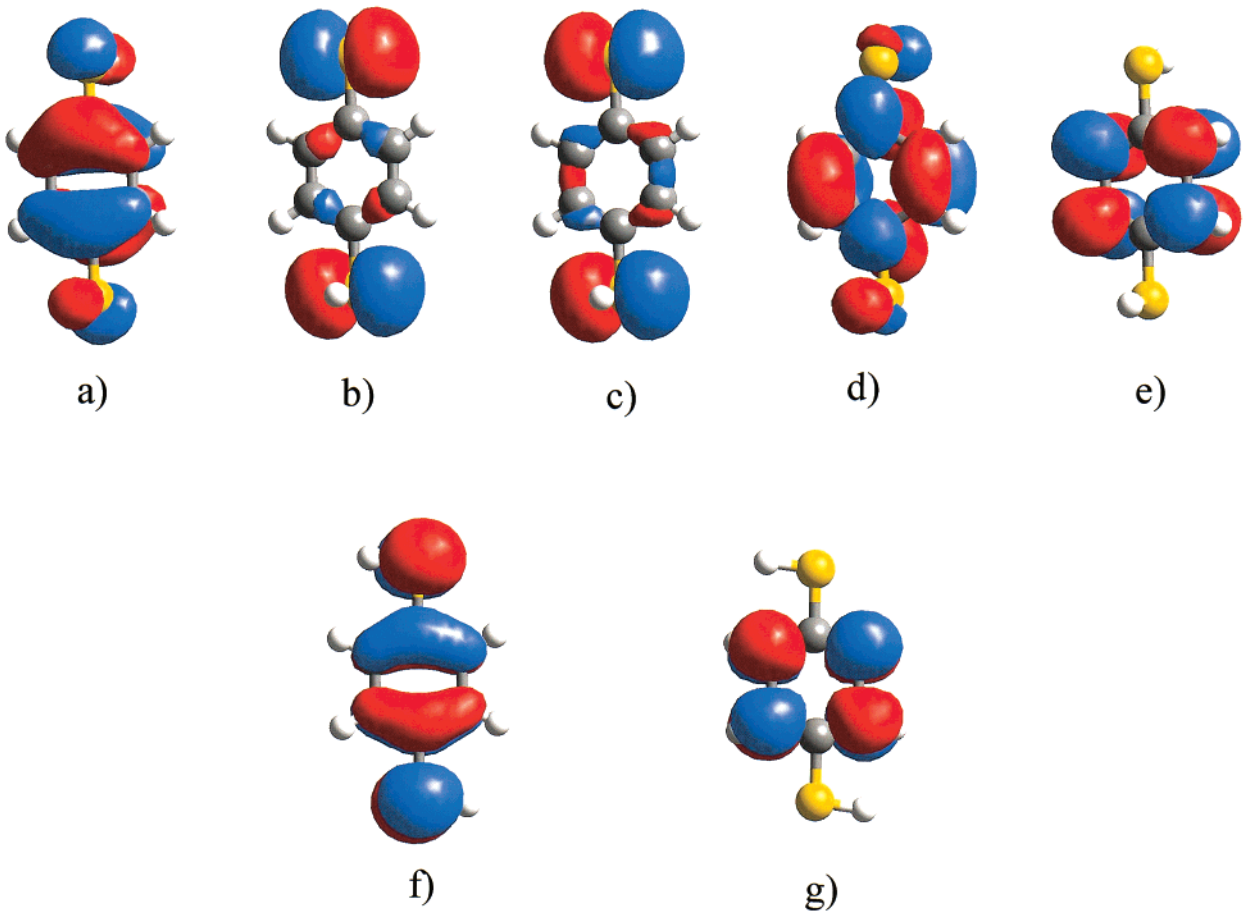

Figure 4. MOs for H−S−(p-C_6H_4)−S−H with the H atoms out of the plane of the ring (**1′**): (a) HOMO-2, (b) HOMO-1, (c) HOMO, (d) LUMO, and (e) LUMO+1, and with H atoms on the plane of the ring (**2′**): (f) HOMO and (g) LUMO.

broadening of these two MOs, they overlap for certain energies and are simultaneously accessible by electrons with energies in the overlap range. The small coupling to the Au atoms yields a narrower DOS peak for the first H_M orbital (MO 42) than for the second (MO 41); therefore, the peak overlap takes place at energies very close to the first H_M orbital. This peak overlap (as opposed to MO overlap, which is zero) explains the high conductance observed at those energies.

The next two H_M orbitals, leading to the next two DOS peaks, are the consequence of a mixture of MOs 43−45. The first of these two DOS peaks is very narrow as a consequence of an orbital localized in the molecule and with low coupling to the Au. The magenta curve indicates that most of the orbital is concentrated on the S atoms. The second peak (located at about −6 eV) is slightly wider than the first one, indicating a H_M orbital with stronger coupling to Au. The integral under these two peaks roughly shows that the contribution to the DOS from the S atoms is 54% and 60% for the first and second peaks, respectively. The transmission function shows that the first peak shows better transmission function than the second one, despite its weaker coupling. This indicates that the delocalization of the orbital around the molecule leading to a higher DOS is a stronger factor for transmission than its coupling to the Au atoms.

Notice that the HOMO and HOMO-1 of **1'** (Figures 4b and c) have strong resemblance to MO 45. Whereas the HOMO-2 (Figure 4a) of **1'** has resemblance to MOs 43 and 44, which have additional contributions from the Au atoms. Therefore, the first peak can be assigned to MOs 43 and 44 because their more delocalized nature in the molecule goes along with the higher DOS of this peak. On the other hand, the second peak would be assigned to MO 45; however, the area below the DOS and the S local DOS curves shows that the orbital related to the second peak should be made of a 60% contribution from S. Contrary to this, the population analysis from Table 1 indicates that MO 45 is made practically of 94% S when ignoring the contribution from the Au atoms. Therefore we can conclude that a strong mixing has occurred to the MOs 43−45 in order to form the two H_M orbitals.

Three peaks connected to MOs 48−53 are observed in the DOS for energies above μ. MOs 50 and 51, mainly localized in the Au atom, yield the second peak, which has a low DOS and transmission function. MOs 48 and 53 (Figure 2) are a mixture of LUMO+1 of the isolated molecule (Figure 4e) with some Au p-character. MO 48 mainly resembles the isolated molecule, whereas MO 53 resembles the Au AOs. On the other hand, MO 49 corresponds to the isolated molecule LUMO combined with some Au p AOs. When the molecule is attached to a macroscopic contact, there is further mixing between its isolated MOs and the Au AOs; therefore, the two H_M orbitals originated from the KS MOs 48, 49, and 53 show perceptible contribution from the LUMO and LUMO+1 of the isolated molecule (Figure 4). The first peak in the DOS at about −1.8 eV shows stronger coupling than the third one at −0.1, yielding a wider and shorter peak. MO 52 is made of 98% from Au AOs; therefore, it contributes neither to the DOS nor to the

transmission function. The assignment of the next higher energy peaks is difficult, but their quantitative estimations may be meaningless due to the limitations of this or any method to deal with virtual MOs.

Results for **2** are shown in Figure 3 and Table 2. The first H_M orbital at −10.4 eV corresponds to MO 28 with some contribution from MO 27. This H_M orbital yields a very shallow region resulting from a peak washed out by its two adjacent large peaks in the DOS. The magnitude of its DOS is due to a very strong coupling between the Au atoms and the molecule. The mixed character of this H_M orbital, made of MO 27 and 28, yields very large values of the transmission function and provides an excellent channel for conduction. The next peak in the DOS at −9.4 eV is formed by three H_M orbitals related to MOs 29 to 32. The main contribution to these MOs comes from the Au atoms, even though MOs 30 and 32 are more evenly distributed than the others are (Table 2). MOs 29−32 yield the highest DOS and transmission function in Figure 3 because of the additive contributions from the three H_M eigenvectors; however, each individual orbital in this peak is expected to have low transmission function. The next H_M orbital at −9.1 eV is mainly MO 33. This MO is over 86% Au and thus its contributions to the DOS and to the transmission function are very small.

The next DOS peak at −8 eV has a small shoulder on its upper energy side, and it involves three H_M orbitals related to MOs 34, 39, and 40. These three H_M orbitals have strong coupling to the Au atoms yielding wide DOS peaks that form a very wide channel for conduction with high transmission function. The contribution of MOs 34 and 39 yields the peak in the transmission function observed at −8 eV and MO 40 yields the shoulder in the DOS (observed as a shallow region in the transmission function) that broadens the conduction channel. MOs 35−38 with over 99% Au contribution (except MO 36 with 92% Au contribution) are not contributing to the DOS (Table 2). MOs 41 and 42 yield the next H_M orbital. These MOs are mainly localized on the S and on the Au atoms (Table 2) with very small contribution from the ring atoms. Their contribution to the DOS is also small; however, due to their coupling to the Au atoms, they contribute significantly to the transmission function extending the shoulder produced by the H_M orbital connected to MO 40.

MOs 43 and 44 yield the next two H_M orbitals. The first one is located at the center of a peak, suggesting an orbital with high localization on the ring, which corresponds to a MO such as 43; however, the width of the peak indicates some coupling to the Au atoms. The projected DOS over the S is also high for these energies indicating high contribution of S AOs as in MO 44. Most likely, this H_M orbital has similar distribution as MO 44, but with some additional contributions from MO 43 that reinforce the delocalization of the ring. The second H_M orbital yields a small shoulder at the upper energy side of the peak. This is another case where two channels of conduction reinforce each other to yield a peak with high transmission function.

Similar to the comparison done between the orbitals of **1** and **1′**, the last of the occupied peaks in the DOS of **2** (for energies smaller than μ) is related to its HOMO (MO 45). This MO also corresponds to the HOMO of the isolated molecule **2′** (Figure 4f) in which H atoms are used instead of the Au atoms. This orbital has π character and it is completely delocalized around the benzene ring and the sulfur. It is also associated with the HOMO-2 of **1′** (Figure 4a). Replacing the H atoms with one Au atom at each side mixes the HOMO, HOMO-1, and HOMO-2 in **1′** giving rise to three MOs. The first one (MO 45) is related to the HOMO and HOMO-1, and the other two (MOs 43 and 44) are related to the HOMO-2 (Figure 2). These three MOs are spread out in an energy range of 0.18 eV, which is much shorter than the 0.5 eV energy separation of the HOMO, HOMO-1, and HOMO-2 of **1′**. Coupling **1** to semi-infinite metallic contacts mix them further leading to two H_M orbitals separated by 0.72 eV. Therefore, the highest-occupied H_M orbital has a strong influence from the π orbital, which is the first available for conduction, and it becomes the HOMO of the molecule when attached to the metallic contacts. On the other hand, this π-orbital is the HOMO of **2** even if we add either one or an infinite number of Au atoms.

Notice that HOMO and HOMO-1 in **1′** shift from −7 eV and −7.13 eV, respectively to −6.56 eV forming MO 45 in **1**. The HOMO-2 located at −7.48 eV yields MO 43 and 44 at −6.74 eV and −6.62 eV, respectively. When coupled with semi-infinite contacts they combine to form an orbital at −6.02 eV giving rise to the highest-occupied H_M orbital. The HOMO of **2′** is located at −5.98 eV. When the molecule is attached to one Au atom at each side (**2**), its HOMO energy shifts to −5.61 eV; but when bonded to the contacts, this level shifts to −5.85 eV, which is very close to the −6.02 eV obtained for the nonplanar configuration. For the out-of-plane cases this π orbital tends to shift up in energy and eventually becomes the HOMO of the molecule when it is attached to Au atoms. However its final energy seems independent of the conformation of the isolated molecule. This is in agreement with Sanderson's principle of electronegativity equalization,[46,47] "when two electronic systems are brought into contact, their chemical potential would tend to align with each other"[48] as implied from the proof of this concept.[49,50] For our particular case, we observe that the HOMO of **1′** and **2′** differ in energy by more than 1 eV and when they are attached to the infinite contacts, they only differ by 0.17 eV indicating that they tend to align to each other along the Fermi level of the macroscopic contacts.

Three peaks are observed for energies above μ for **2**. The first one corresponds to orbitals 48 and 49, the second to 50 and 51, and the third to 53. In this case, the presence of the Au atom on the ring plane eliminates the σ plane of symmetry perpendicular to the ring plane that exists in **1**, making the mixing of the LUMO of **2′** with the Au AOs more complex than in the case of molecule **1**. MOs 48, 50, and 53 look like the LUMO of **2′** (Figure 4g), which is similar to the LUMO+1 of **1′**.

Figure 5 shows the $I-V$ (eq 5) and the $g-V$ (eq 7) curves for **1** (red curve) and **2** (green curve), as well as the experimental curve (gray curve).[4] The close agreement between theory and experiment is encouraging, especially for the current that shows much less noise than the conductance. The current is also similar to other ab initio results where a constrained D_{2h} symmetry was used (i.e., a C−S−Au angle of 180°).[5] The differential conductance for **1** and **2** shows a plateau for low voltage (less than 1 V) that establishes a threshold for conduction. After this threshold, the differential conductance reaches a maximum due to the HOMO, and therefore increasing the current. The position of the first peak in **1** and **2** in the conductance curves differs by 0.38 V. Since a potential difference of ΔV in the $I-V$ or $g-V$ curves corresponds to a $\Delta E = 1/2\ e\ \Delta V$ in the DOS−energy and transmission function−energy curves, the 0.17 eV difference between the positions of the corresponding H_M orbitals is in perfect agreement with the conductance results. This first peak in the $g-V$ is higher for **1** than for **2** as it is reflected in their transmission functions shown in Figures 2 and 3, respectively. We can infer that the nonplanar configuration (**1**) favors the

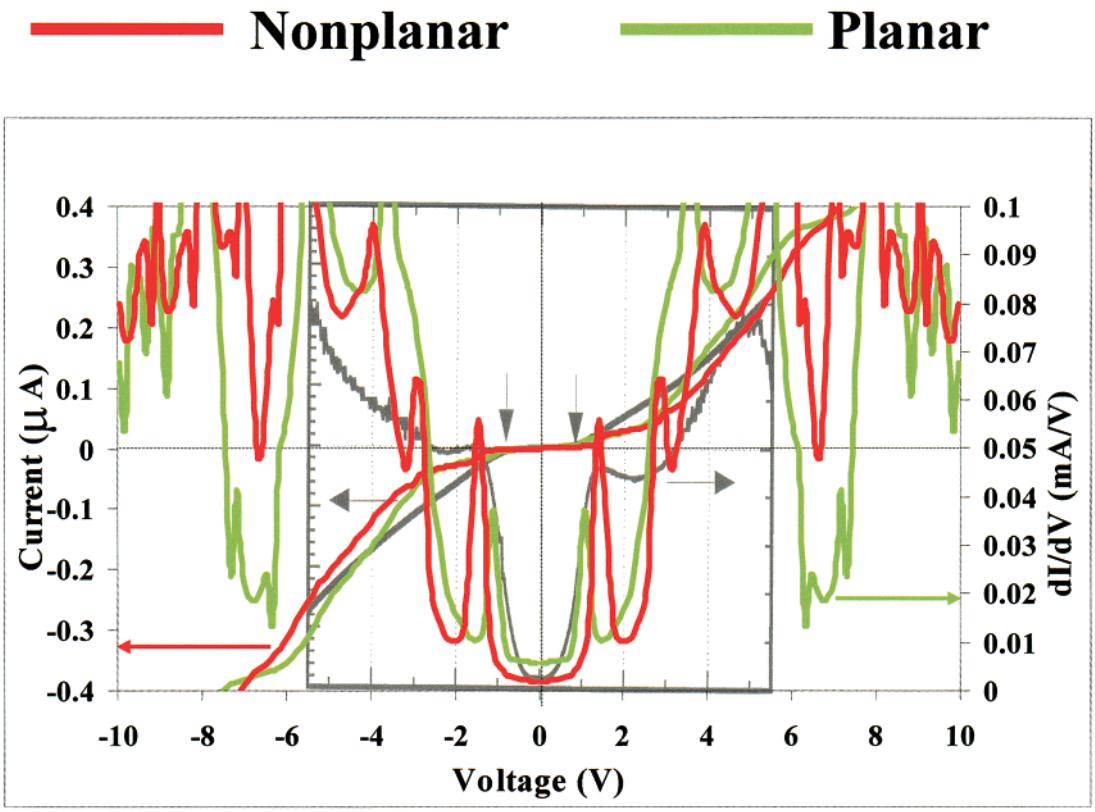

Figure 5. $I-V$ for **1** (red curves), **2** (green curves), and experimental results (gray curves). Adapted from the experimental report.[4]

bonding to the Au, as indicated by its wider first peak in the DOS and transmission function (Figure 2) when compared to the first peak in the DOS and transmission function of **2** (Figure 3). The differential conductance features, up to a voltage of 7 V, can be directly associated to the transmission function for energies below μ. However, at about 7 V, the virtual orbitals become available and the differential conductance is determined by the joint effect of the empty and occupied orbitals located 3.5 eV above and below μ. Notice that the $I-V$ curve is what should be compared to the experiment, and they are in excellent agreement. We have used the $g-V$ curves obtained as calculated directly from our $I-V$ curves. These are different to the one obtained from the experiment where a finite averaging is involved when estimating the derivatives. If the step size of the derivation is increased, a curve similar to the experimental one will eventually be obtained (not showed), which washes out several interesting features of the differential conductance.

We have not considered the explicit effect of vibrational modes; however, calculations, using a semiempirical self-consistent approach proposed by Datta,[28] show changes of 1% in the current. Work is in progress for an ab initio consideration of the vibrational modes on the transport characteristics.

The effect of the bias field on the system is included implicitly in the Green function formalism; however it is not included in the Hamiltonian defining the molecule. Calculations performed in a fully self-consistent manner whereas the Hamiltonian changes as the bias field changes show current deviations in the order of 3% for the systems treated in this work. However, we found strong effects for other molecules.[51,52]

Figure 6a,b shows the $I-V$ and $g-V$, respectively for the six systems containing Au. Notice that **3**, **4**, and **6**, which have 2, 3, and 5 Au atoms at each end, respectively, yield thresholds for conduction of over 3 V and the first peak in the differential conductance takes place at about 4 V (Figure 6b). This peak is due to the HOMO of the molecule, which is shifted 1.5 eV or more with respect to its position in **1** and **2**. Since there are two Au atoms bonded to the S atom instead of just one in **3**, **4**, and **6**, we can conclude that 1,4 benzene-dithiolate conducts better when the S atom is attached directly to just one Au atom rather than to two or more. We suggest that this is the case of the reported break junction experiment due to the almost perfect matching of the $I-V$ curves with the experimental one.[4] In addition, **5** corroborates the above because it has four Au atoms at each end, but the S is only bonded to one Au atom. Therefore, the first peak in the differential conductance takes place at voltages similar to those of **1**, **2**, and **5** that are the only other cases where each S atom attaches directly to one Au atom. The peak in the differential conductance of **5** related to the HOMO is small but able to determine a conduction threshold of less than 1 V.

The possibility of the S atom being bonded to a hollow site of a triangle of Au atoms can also be discarded from our present results. The Au−S bond lengths obtained for all the cases with our DFT calculations are between 2.51 and 3.37 Å and the angle C−S−Au between 102° and 108°. If an S atom is bonded to the center of Au triangle (the typical Au−Au length in the (111) Au surface is 2.88 Å) with an Au−S length of 2.45 Å, the angle C−S−Au would be of 137°. If instead we try to conserve the typical C−Au−S angle of 105°, the Au−S distance would have to be 1.72 Å. Therefore, the hollow position for the S atom would create a high-energy and strain system. Indeed, none of the systems we tried in addition to those reported here converged to a configuration with more than two Au atoms directly bonded to the S atoms. Notice that μ is not used as an adjustable parameter, since different values of μ would have changed the extension of the threshold in the $I-V$ curves, making it

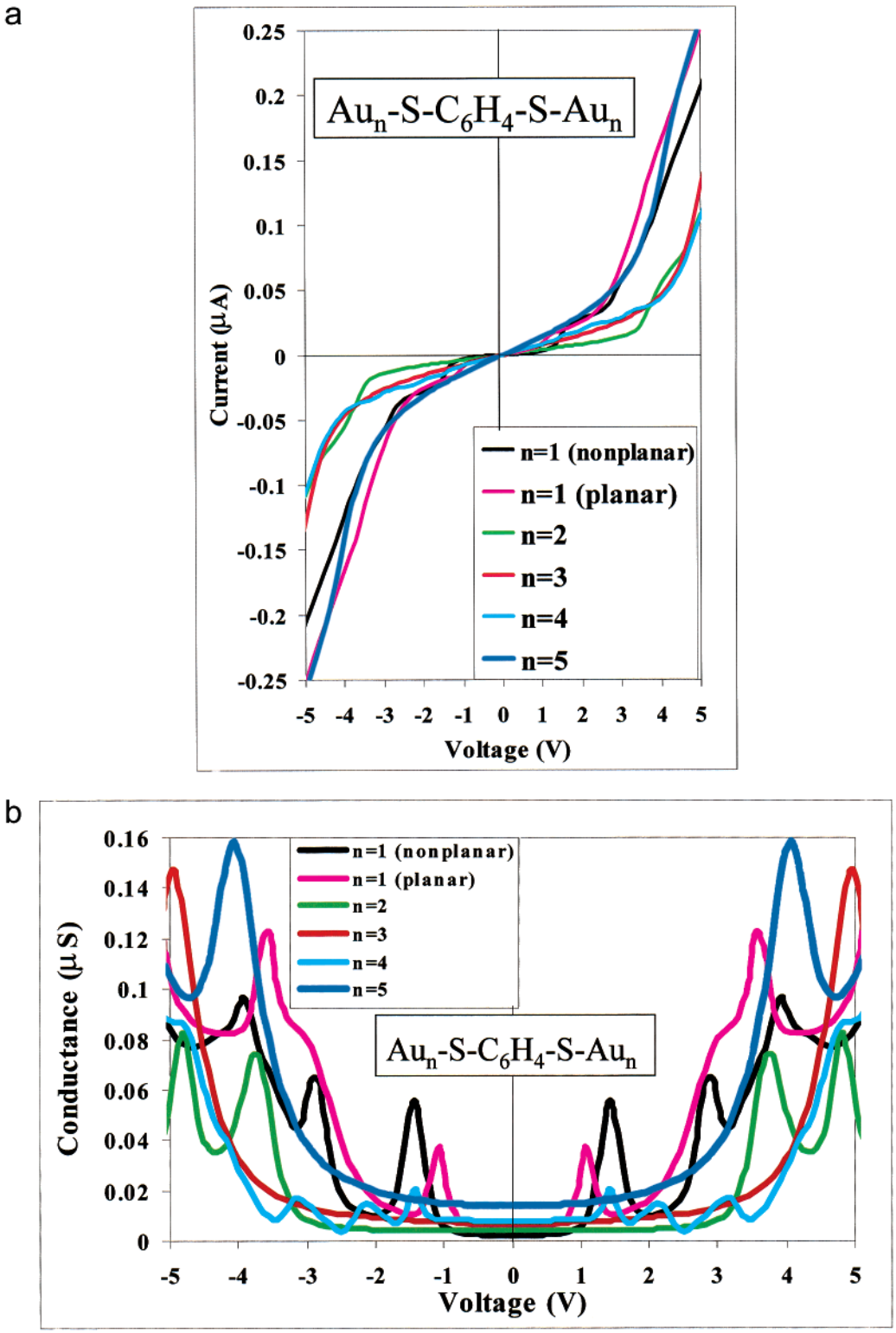

Figure 6. (a) $I-V$, and (b) $g-V$ for **1**−**6**.

impossible to determine which of the ab initio geometries corresponds to the experiment. μ corresponds to the experimental work function for the (111) surface of Au.

Conclusions

We have combined Green functions and density functional formalisms in order to study electronic conduction in molecules addressed by two macroscopic tips. We showed that the KS MOs are indicators of the conductance characteristics through single molecules, allowing us to infer the composition of the H_M orbitals. The characteristics of the H_{KS} relate to the details of the DOS and transmission function, explaining the conductance features of the metal−molecule−metal junction from the characteristics of the isolated molecule. It is shown that delocalized orbitals show better transmission function than localized ones. Collective effects among MOs were observed and they are responsible for unusual features in the transmission function. One of these cases is when two or more MOs of the

isolated molecule spatially localized in different parts combine, and they yield a conduction channel with high transmission function. This is a direct consequence of the broadening of the MOs because their interaction with the continuum levels of the contacts. The coupling to the Au contact shifts the electronic levels of the molecule in order to align them with the Fermi level of the unbiased Au contacts. However, the molecular levels do not shift in a concerted manner among them because the strong mixing of the isolated MOs. The features of one particular KS orbital can be found in two or more H_M orbitals. Particularly there is a π orbital delocalized on the ring and S atoms that becomes the HOMO and it is the first orbital available for conduction independently of its position relative to the other molecular orbitals in the isolated molecule. The energies of these special MOs in the isolated molecules can vary from isomer to isomer; however, they will try to align to the same energy, as indicated by their corresponding H_M eigenvalues, when the isomers are connected to metallic atoms. The energy of these H_M orbitals with respect to μ always determines the threshold for conduction. Due to the low density of unoccupied states close to μ and the different shift of occupied and unoccupied MOs, the transport of electrons takes place first through the occupied channels for this particular class of systems. The experimental set up corresponds to the case of the molecule connected directly to a single Au atom at each side.[4] The direct connection to two Au atoms would yield a much larger threshold than the one obtained in the experiment and the direct connection to 3 or more Au atoms is ruled out by geometrical considerations. Therefore, 1,4 benzene-dithiolate attaches to two junctions by bonding directly to just one Au atom on each side as in **1** or **2**.

Acknowledgment. We highly appreciate the support of DARPA/ONR under Grant N00014-99-1-0406, ARO under Grants DAAD19-00-1-0154 and DAAD19-99-1-0085, and the supercomputer support of NASA. We also appreciate discussions with John Perdew and Michael Frisch, as well as with Supriyo Datta and his group who provided details of their *MolecularIV* program.

References and Notes

(1) Ellenbogen, J. C.; Love, J. C. *Proc. IEEE* **2000**, *88*, 386−426, and references therein.
(2) Margaritondo, G. *Rep. Prog. Phys.* **1999**, *62*, 765−808.
(3) Peressi, M.; Binggeli, N.; Baldereschi, A. *J. Phys. D.: Appl. Phys.* **1998**, *31*, 1273−1299.
(4) Reed, M. A.; Zhou, C.; Muller, C. J.; Burgin, T. P.; Tour, J. M. *Science* **1997**, *278*, 252−254.
(5) Seminario, J. M.; Zacarias, A. G.; Tour, J. M. *J. Phys. Chem. A* **1999**, *103*, 7883−7887.
(6) Yazdani, A.; Eigler, D. M.; Lang, N. D. *Science* **1996**, *272*, 1921−1924.
(7) Olesen, L.; Lægsgaard, E.; Stensgaard, I.; Besenbacher, F.; Schiøtz, J.; Stoltze, P.; Jacobsen, K. W.; Nørskov, J. K. *Phys. Rev. Lett.* **1994**, *72*, 2251−2254.
(8) Pascual, J. I.; Méndez, J.; Gómez-Herrero, J.; Baró, A. M.; García, N. *Phys. Rev. Lett.* **1993**, *71*, 1852−1855.
(9) Agraït, N.; Rodrigo, J. G.; Vieira, S. *Phys. Rev. B* **1993**, *47*, 12345−12348.
(10) Chen, J.; Calvet, L. C.; Reed, M. A.; Carr, D. W.; Grubisha, D. S.; Bennett, D. W. *Chem. Phys. Lett.* **1999**, *313*, 741−748.
(11) Zhou, C.; Deshpande, M. R.; Reed, M. A.; Jones, L., II; Tour, J. M. *Appl. Phys. Lett.* **1997**, *71*, 611−613.
(12) Seminario, J. M.; Zacarias, A. G.; Tour, J. M. *J. Am. Chem. Soc.* **1998**, *120*, 3970−3974.
(13) Lang, N. D. *Phys. Rev. B* **1995**, *52*, 5335−5342.
(14) Lang, N. D. *Phys. Rev. Lett.* **1997**, *79*, 1357−1360.
(15) Lang, N. D. *Phys. Rev. B* **1997**, *55*, 9364−9366.
(16) Ventra, M. D.; Pantelides, S. T.; Lang, N. D. *Phys. Rev. Lett.* **2000**, *84*, 979−982.
(17) Samanta, M. P.; Tian, W.; Datta, S.; Henderson, J. I.; Kubiak, C. P. *Phys. Rev. B* **1996**, *53*, R7626−R7629.
(18) Yaliraki, S. N.; Ratner, M. A. *J. Chem. Phys.* **1998**, *109*, 5036−5043.
(19) Yaliraki, S. N.; Kemp, M.; Ratner, M. A. *J. Am. Chem. Soc*. **1999**, *121*, 3428−3434.
(20) Mujica, V.; Kemp, M.; Roitberg, A.; Ratner, M. *J. Phys. Chem.* **1996**, *104*, 7296−7305.
(21) Balbuena, P. B.; Derosa, P. A.; Seminario, J. M. *J. Phys. Chem. B* **1999**, *103*, 2830−2840.
(22) Datta, S. *Electronic Transport in Mesoscopic Systems*; Cambridge University Press: Cambridge, U.K., 1995.
(23) Datta, S.; Tian, W.; Hong, S.; Reifenberger, R.; Henderson, J.; Kubiak, C. P. *Phys. Rev. Lett.* **1997**, *79*, 2530−2533.
(24) Kemp, M.; Mujica, V.; Ratner, M. A. *J. Chem. Phys.* **1994**, *101*, 5172−5178.
(25) Mujica, V.; Kemp, M.; Ratner, M. A. *J. Chem. Phys.* **1994**, *101*, 6849−6855.
(26) Mujica, V.; Kemp, M.; Ratner, M. A. *J. Chem. Phys.* **1994**, *101*, 6856−6864.
(27) Hall, L. E.; Reimers, J. R.; Hush, N. S.; Silverbrook, K. *J. Chem. Phys.* **2000**, *112*, 1510−1521.
(28) Tian, W.; Datta, S.; Hong, S.; Reifenberger, R.; Henderson, J. I.; Kubiak, C. P. *J. Chem. Phys.* **1998**, *109*, 2874−2882.
(29) Yaliraki, S. N.; Roitberg, A. E.; Gonzalez, C.; Mujica, V.; Ratner, M. A. *J. Chem. Phys.* **1999**, *111*, 6997−7002.
(30) Emberly, E. G.; Kirczenow, G. *Phys. Rev. B* **1998**, *58*, 10911−10920.
(31) Papaconstantopoulos, D. A. *Handbook of the Band Structure of Elemental Solids*; Plenum Press: New York, 1986.
(32) Tian, W.; Samanta, M.; Xue, Y.; Zahid, F.; Datta, S. *MolecularIV*, unpublished.
(33) Frisch, M. J.; Trucks, G. W.; Schlegel, H. B.; Gill, P. M. W.; Johnson, B. G.; Robb, M. A.; Cheeseman, J. R.; Keith, T.; Petersson, G. A.; Montgomery, J. A.; Raghavachari, K.; Al-Laham, M. A.; Zakrzewski, V. G.; Ortiz, J. V.; Foresman, J. B.; Cioslowski, J.; Stefanov, B. B.; Nanayakkara, A.; Challacombe, M.; Peng, C. Y.; Ayala, P. Y.; Chen, W.; Wong, M. W.; Andres, J. L.; Replogle, E. S.; Gomperts, R.; Martin, R. L.; Fox, D. J.; Binkley, J. S.; Defrees, D. J.; Baker, J.; Stewart, J. P.; Head-Gordon, M.; Gonzalez, C.; Pople, J. A. *Gaussian 94*, revision E.1; Gaussian, Inc.: Pittsburgh, PA, 1996.
(34) Frisch, M. J.; Trucks, G. W.; Schlegel, H. B.; Scuseria, G. E.; Robb, M. A.; Cheeseman, J. R.; Zakrzewski, V. G.; Montgomery, J. A., Jr.; Stratmann, R. E.; Burant, J. C.; Dapprich, S.; Millam, J. M.; Daniels, A. D.; Kudin, K. N.; Strain, M. C.; Farkas, O.; Tomasi, J.; Barone, V.; Cossi, M.; Cammi, R.; Mennucci, B.; Pomelli, C.; Adamo, C.; Clifford, S.; Ochterski, J.; Petersson, G. A.; Ayala, P. Y.; Cui, Q.; Morokuma, K.; Malick, D. K.; Rabuck, A. D.; Raghavachari, K.; Foresman, J. B.; Cioslowski, J.; Ortiz, J. V.; Stefanov, B. B.; Liu, G.; Liashenko, A.; Piskorz, P.; Komaromi, I.; Gomperts, R.; Martin, R. L.; Fox, D. J.; Keith, T.; Al-Laham, M. A.; Peng, C. Y.; Nanayakkara, A.; Gonzalez, C.; Challacombe, M.; Gill, P. M. W.; Johnson, B. G.; Chen, W.; Wong, M. W.; Andres, J. L.; Head-Gordon, M.; Replogle, E. S.; Pople, J. A. *Gaussian 98*, revision A.9; Gaussian, Inc.: Pittsburgh, PA, 1998.
(35) Becke, A. D. *J. Chem. Phys.* **1993**, *98*, 5648−5652.
(36) Perdew, J. P.; Chevary, J. A.; Vosko, S. H.; Jackson, K. A.; Pederson, M. R.; Singh, D. J.; Fiolhais, C. *Phys. Rev. B* **1992**, *46*, 6671−6687.
(37) Perdew, J. P.; Wang, Y. *Phys. Rev. B* **1992**, *45*, 13244−13249.
(38) Wadt, W. R.; Hay, P. J. *J. Chem. Phys.* **1985**, *82*, 284−298.
(39) Hay, P. J.; Wadt, W. R. *J. Chem. Phys.* **1985**, *82*, 270−283.
(40) Hay, P. J.; Wadt, W. R. *J. Chem. Phys.* **1985**, *82*, 299−310.
(41) Seminario, J. M.; Zacarias, A. G.; Tour, J. M. *J. Am. Chem. Soc.* **1999**, *121*, 411−416.
(42) Zacarias, A. G.; Castro, M.; Tour, J. M.; Seminario, J. M. *J. Phys. Chem. A* **1999**, *103*, 7692−7700.
(43) Seminario, J. M.; Zacarias, A. G.; Castro, M. *Int. J. Quantum Chem.* **1997**, *61*, 515−523.
(44) *CRC Handbook of Chemistry and Physics*; Lide, D. R., Eds.; CRC Press: Boca Raton, Fl, 1998.
(45) Mulliken, R. S. *J. Chem. Phys.* **1955**, *23*, 1833−1841. Mulliken, R. S. *J. Chem. Phys.* **1955**, 23, 2338−2343.
(46) Sanderson, R. T. *Science* **1951**, *114*, 670−672.
(47) Sanderson, R. T. *Chemical Bonds and Bond Energy*, 2nd. ed.; Academic Press: New York, 1976.
(48) Parr, R. G.; Yang, W. *Density Functional Theory of Atoms and Molecules*; Oxford University Press: Oxford, 1989.
(49) Parr, R. G.; Donnelly, R. A.; Levy, M.; Palke, W. E. *J. Chem. Phys.* **1978**, *68*, 3801−3807.
(50) Politzer, P.; Weinstein, H. *J. Chem. Phys.* **1979**, *71*, 4218−4220.
(51) Seminario, J. M.; Zacarias, A. G.; Derosa, P. A. *J. Phys. Chem. A*, in press.
(52) Seminario, J. M.; Zacarias, A. G.; Derosa, P. A. *J. Chem. Phys.*, submitted.